ACS APPLIED MATERIALS & INTERFACES

Research Article

www.acsami.org

Enhanced Reactive Adsorption of Hydrogen Sulfide on the Composites of Graphene/Graphite Oxide with Copper (Hydr)oxychlorides

Oluwaniyi Mabayoje, Mykola Seredych, and Teresa J. Bandosz*

Department of Chemistry, The City College of New York, 160 Convent Avenue, New York, New York 10031, United States

ABSTRACT: Composites of copper (hydr)oxychlorides with graphite oxide or graphene were synthesized and used as adsorbents of hydrogen sulfide at dynamic conditions at ambient temperatures. The materials were extensively characterized before and after adsorption in order to link their performance to the surface features. X-ray diffraction, FTIR, thermal analysis, TEM, SEM/EDX, and adsorption of nitrogen were used. It was found that the composite with graphene has the most favorable surface features enhancing reactive adsorption of hydrogen sulfide. The presence of moisture in the H_2S stream has a positive effect on the removal process owing to the dissociation process. H_2S is retained on the surface via a direct replacement of OH groups and via acid−base reactions with the copper (hydr)oxide. Highly dispersed reduced copper species on the surface of the composite with graphene enhance activation of oxygen and cause formation of sulfites and sulfates. Higher conductivity of the graphene phase than that of graphite oxide helps in electron transfer in redox reactions.

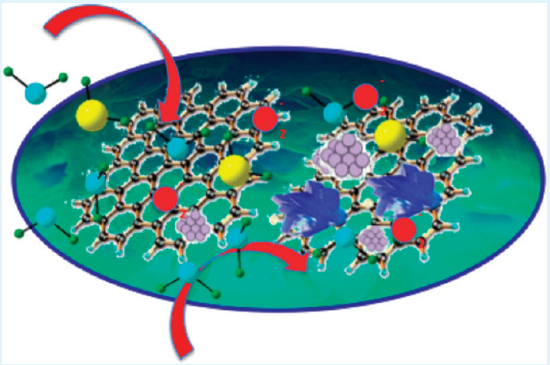

KEYWORDS: *graphite oxide, graphene, copper (hydr)oxychlorides, composites, H_2S adsorption, reactive adsorption*

INTRODUCTION

Graphite oxide (GO) has recently emerged as a material of interest especially because of its potential as a precursor in the bulk and inexpensive production of single sheet graphene.[1] The ability to modify it and to build graphite oxide-based composite materials has also been studied in recent times.[2,3] Materials based on graphite oxide and chemically converted graphene have been found to be useful in the area of environmental chemistry especially in the purification of water and in the sensing and removal of toxic gases from the environment. Modified graphite oxides have been studied in the removal of metals from water[4−6] and in the removal of various gaseous air pollutants from the atmosphere.[7−16] Graphene originating materials have also been tested in the removal of ammonia,[7,16] hydrogen sulfide,[8,11] sulfur dioxide,[9,17] or nitrogen oxides.[10,13,15,18] They are advantageous as adsorbents because their physical properties and surface chemistry can be modified to enhance the interactions with target molecules. Furthermore, graphene-based composites with inorganic compounds are expected to show catalytic properties that may be important for the interactions between adsorbents and target molecules. For example, GO/zinc hydroxide composites[19] showed photocatalytic activity significantly enhancing the reactive adsorption of various gases on these materials.[11,17,18] The presence of a graphene-based phase in these materials helped with separation of electrons and holes, preventing their recombination, and contributed to charge transfer because of its electrical conductivity.[19,20]

The removal of toxic gases from the environment has became an important issue in recent times due to an increase in industrial activities and the consequent regulations of the emission of pollutants produced in various industrial processes.[21] There is also a possibility of an accidental release of toxic species to confined spaces with the fatal effect for humans. Such species are referred to as Toxic Industrial Compounds (TICs) and hydrogen sulfide is listed one of them. Besides its natural origin from anaerobic decomposition of an organic matter, H_2S is also produced in industrial activities such as burning of fossil fuels and crude oil processing.

Composites of graphite oxide or graphene with zinc (hydr)oxide have been recently studied as adsorbents of TICs at ambient conditions.[11,17,18] They were reported to remove 20 wt % H_2S, especially when moisture was present in the air and the adsorption was found to be enhanced by the photocatalytic activity of the materials in visible light. The synergetic effect of the GO component was linked to the structure of the composite where the zinc hydr(oxide) component had more terminal groups than in the bulk phase. These groups were shown to take part in oxidation reactions via a photochemical path. The graphite oxide and graphene component were also found to help in an electron transfer leading to oxygen activation. The superiority of the GO composites over those with graphene was linked to the presence of oxygen activating

Received: April 25, 2012
Accepted: May 29, 2012
Published: June 5, 2012

functional groups and bonds with zinc hydr(oxide) in the former materials. Products formed on the surface of the composites as a result of reactive adsorption of H_2S included elemental sulfur, sulfite and sulfate species and zinc sulfide.[11] The enhancement in H_2S reactive adsorption in comparison with the parent materials was also found on the composites of cobalt (hydr)oxide with graphite oxide or graphene.[22] In this case the importance of oxygen groups of cobalt hydroxide/GO composites for the adsorption of hydrogen sulfide was revealed. An activation of oxygen by the carbonaceous component resulted in formation of sulfites. The differences in the performance of $Co(OH)_2$/GO composite with different ratios of components were linked to the availability of active sites on the surface of the adsorbents, dispersion of these sites, their chemical heterogeneity and location in the pore system.

The effects of metal oxides combined with carbonaceous materials on the removal of H_2S has also been studied using activated carbons as a catalyst support.[23] In this group of materials, copper hydroxide-based adsorbents were found as very efficient adsorbents for hydrogen sulfide removal at ambient conditions. Apart from directly reacting with hydrogen sulfide, these species were also found to catalyze the oxidation of hydrogen sulfide on activated carbons.

Besides catalytic oxides on an activated carbon support, mixed oxides were also extensively investigated as H_2S adsorbents at ambient condition.[24,25] Mixed Fe−Mn−Zn−Ti−O metal oxides were shown as efficient environmentally friendly desulfurization adsorbents.[24] Addition of copper as a dopand to ZnO_2-supported on silica significantly increased the utilization of the zinc oxide phase at room temperature.[25] That high efficiency was attributed to nanodispersion of active copper and zinc on the surface of the catalyst. Adsorption of H_2S resulted in reduction of copper from 2+ to 1+, and that reduction degree was correlated with the performance of the adsorbents.[25]

Following this, copper (hydr)oxychlorides/GO and copper (hydr)oxychlorides/graphene composites were synthesized and studied as adsorbents of H_2S in dry and moist conditions at ambient temperatures. The objective of this paper is the evaluation of the role of carbonaceous phase in building the textural and chemical properties of the composites and its effect on the adsorptive properties. The extent of the reactive adsorption of hydrogen sulfide is linked to the surface features with the mechanism of adsorption as a deliverable.

EXPERIMENTAL SECTION

Materials. The composites of GO/copper (hydr)oxychlorides and Gr/copper (hydr)oxychlorides were prepared by dispersing GO powder or graphene (supplied by METSS Corporation (Westerville, OH)) (20 wt % of the final mass of the material) in the 350 mL of copper chloride (0.025 M). The resulting well-dispersed suspension was stirred for 1 h. The sodium hydroxide solution (0.05 M) was then added (350 mL) to the dispersed graphene-based phase with a rate 2.0 mL/min using a Titronic Universal (SCHOTT). Then, the obtained composites were immediately washed with distilled water until neutral pH and no traces of chloride ions were found. Finally, the bluish precipitate formed was filtered and dried at 100 °C for 24 h. Copper (hydr)oxychlorides composites formed with graphite oxide and graphene are referred to as CuGO and CuGr respectively.

For the sake of comparison the commercial nanomaterial, CuO-C, supplied by NanoScale Corporation was also used.

Methods. *H_2S Breakthrough Capacity.* Dynamic tests were carried out at room temperature to evaluate the capacity of the adsorbents for H_2S removal under two sets of conditions: wet and dry. For the former, adsorbent samples were packed into a glass column (length 370 mm, internal diameter 9 mm). A bed volume used was 1.6 cm^3 (with the mass of adsorbent between 0.28 to 0.55 g depends of density our materials studied). Before the experiments in moist air the samples were prehumidified with moist air (relative humidity 70% at 25 °C) for two hours. The amount of water adsorbed was estimated from the increase in the sample weight. Dry or moist air (relative humidity 70% at 25 °C) containing 0.1% (1000 ppm) H_2S was then passed through the column of adsorbent at 500 mL/min. The breakthrough of H_2S was monitored using a MultiRae Plus monitoring system with an electrochemical sensor. The test was stopped at the breakthrough concentration of 100 ppm (sensor limit). The adsorption capacities of each adsorbent in terms of gram of H_2S per gram of adsorbent were calculated by integration of the area above the breakthrough curves, and from the H_2S concentration in the inlet gas, flow rate, breakthrough time, and mass of adsorbent.

FT-IR Spectroscopy. Fourier transform infrared (FT-IR) spectroscopy was carried out using a Nicolet Magna-IR 830 spectrometer using the attenuated total reflectance (ATR) method. The spectrum was generated and collected 32 times and corrected for the background noise. The experiments were done on the powdered samples, without KBr addition.

Thermal Analysis. Thermogravimetric (TG) curves were obtained using a TA Instruments thermal analyzer. The initial and spent samples were exposed to an increase in temperature (10 °C/min) while the nitrogen flow rate was held constant (100 mL/min). From the TG curves, differential TG (DTG), and DTA curves were derived.

Potentiometric Titration. Potentiometric titration measurements were performed with a DMS Titrino 716 automatic titrator (Metrohm). The instrument was set at the mode where the equilibrium pH is collected. Subsamples of the initial and spent materials (~0.100 g) were added to $NaNO_3$ (0.01 M, 50 mL) and placed in a container maintained at 25 °C overnight for equilibrium. During the titration the suspension was continuously saturated with N_2 to eliminate the influence of atmospheric CO_2. The suspension was stirred throughout the measurements. Volumetric standard NaOH (0.1 M) was used as the titrant starting from the initial pH of the materials suspension up to pH 11. The experimental data were transformed into a proton binding curves, Q, representing the total amount of protonated sites.[26,27]

pH of the Surface. A 0.1 g sample of dry adsorbent was added to 5 mL of deionized water and the suspension was stirred overnight to reach equilibrium. The pH of suspension was measured using an Accumet Basic pH meter (Fisher Scientific, Springfield, NJ, USA).

SEM/EDX. Scanning electron microscopy images were obtained using a Zeiss Supra 55 VP with an accelerating voltage of 15.00 kV. Scanning was performed in situ on a sample powder previously dried (120 °C). SEM images with energy-dispersive X-ray (EDX) analysis were done at 10 KX magnifications.

TEM. Transmission electron microscopy (TEM) was performed on a Zeiss EM 902 instrument. The microscope has a line resolution of 0.34 nm and a point resolution of 0.5 nm; operates in normal, diffraction and low dose modes at 50 or 80 kV. Analyses were done after the sample was resuspended in ethanol.

Nitrogen Adsorption. N_2 isotherms were measured at −196 °C using an ASAP 2020 (Micromeritics, Surface area and porosity analyzer Norcross, GA, USA). Prior to each measurement, initial and spent samples were outgassed at 120 °C to vacuum 1×10^{-4} Torr. The surface area, S_{BET}, (Brunauer−Emmet−Teller method was used), the micropore volume, V_{mic}, (calculated using the Dubinin−Radushkevich approach)[28] the mesopore volume, V_{mes}, the total pore volume, V_t, (calculated from the last point of the isotherms based on the volume of nitrogen adsorbed) were calculated from the isotherms. The volume of mesopores, V_{mes}, represents the difference between total pore and micropore volume.

X-ray Diffraction (XRD). XRD measurements were conducted using standard powder diffraction procedures. Adsorbents were ground with methanol in a small agate mortar. The mixture was smear-mounted and then analyzed by Cu K_α radiation generated in a Phillips X'Pert X-ray diffractometer to obtain diffraction peaks of samples. A standard glass slide was run for the background.

RESULTS AND DISCUSSION

The measured breakthrough curves on the commercial copper oxide and the composites are collected in Figure 1. The steep

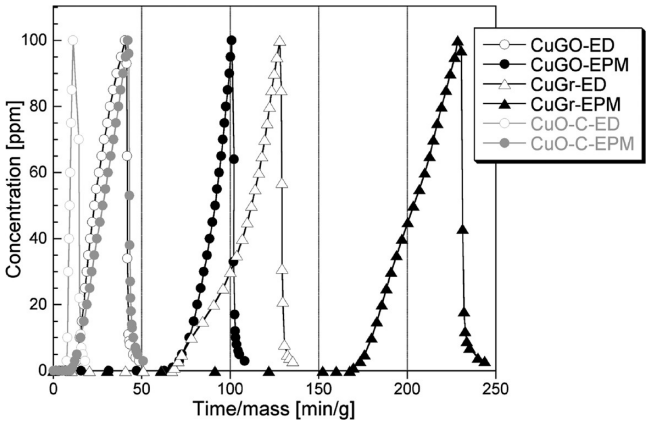

Figure 1. H_2S breakthrough curves measured in dry (ED) and moist (EPM) conditions on the materials studied.

desorption curves indicate strong adsorption of H_2S. No SO_2 was detected in the outlet gas during the duration of the experiment. Even though the shapes of the breakthrough curves are similar, the slopes of those run in moist air are slightly less steep, which suggests different kinetics of the reactive adsorption, related to the mechanism of surface reactions. Apparently, the surface is reactive and it was seen by the change of the color of the composites in the column from greenish to black during running the breakthrough tests, which suggested formation of sulfides.

The calculated breakthrough capacities, the amount of water preadsorbed during prehumidification, and the surface pH values are collected in Table 1. The presence of moisture

Table 1. H_2S Breakthrough Capacities, Amount of Water Preadsorbed, and the Surface pH Values for the Materials Studied

	H_2S breakthrough capacity			pH	
sample[a]	(mg/g)	(mg/cm^3)	H_2O adsorbed (mg/g)	In	Exh
CuGO-ED	27.5	5.9		5.67	5.54
CuGO-EPM	70.5	28.2	16.9	5.67	5.12
CuGr-ED	42.7	9.4		5.69	5.61
CuGr-EPM	159.8	42.0	41.9	5.69	5.47
CuO-C-ED	7.7	3.4		8.33	8.31
CuO-C-EPM	28.7	13.3	41.6	8.33	8.29

[a]ED refers to the experiments run in dry air; EPM, in moist air after pre-humidification.

increases the capacity from two to three folds. This effect is expected taking into account that the acid−base reactions are favored in the dissociated state. Moreover, it is also well-known that for hydrogen sulfide oxidation dissociation to HS^- is a critical step.[29] Interestingly, in both dry and moist conditions the composite with graphene is the best adsorbent with three times more hydrogen sulfide adsorbed in moist conditions compared to the dry ones. When CuGr is compared to CuGO, the former has twice better performance. The composites visibly outperform GO and Gr on which the capacity was negligible, copper (hydr)oxychlorides and commercial nanosize copper oxide. Even though the amount of water preadsorbed on CuO and CuGr are similar, the capacity of the latter is 300% higher than the former. That relatively high affinity of the CuGr to adsorb water was not expected taking into account the hydrophobic character of the graphene phase. This behavior can contribute to the adsorptive performance. The chemistry and the texture of the copper (hydr)oxychlorides phase is expected to affect this behavior.

On the basis of the average surface pH values listed in Table 1, the composites are much more acidic than commercial CuO. Although the addition of 20% of GO of surface pH 2.5[7] can somehow contribute to the low pH of the composite with the more basic (hydr)oxychlorides component, it cannot be in the case for graphene (pH 5.6). Therefore, new chemistry of the composites might be one of the factors contributing to the measured acidity. Another possibility is the presence of chlorides (discussed below), which,as Lewis acids, can get protonated in the water phase. Because copper species are known to activate oxygen,[30,31] we cannot cross out the possibility of the graphene phase oxidation in situ in the composite. This phase should be much more susceptible to oxidation than oxygen saturated GO. This process could explain the high affinity of the CuGr to retain water. Nevertheless, the amount adsorbed on the composites is much higher than that on CuO-C, in spite of the favorable surface pH (8.3) of the latter. After H_2S adsorption, the pH is practically unchanged, which suggests the formation of either sulfur or sulfur containing copper salts.

The TEM images for our materials are collected in Figure 2. The CuO−C shows the small aggregates of copper oxide nanoparticles. In the case of composite with GO the thin layer of graphene oxide is seen with the very small uniform particles of the copper phase. The particle distribution seems to be very homogeneous. The deposition of copper (hydr)oxychlorides particles with sizes of about 5−10 nm likely happens in the vicinity of oxygen groups on the basal planes of graphite layers.[32] These groups might work as anchoring sites for the deposition of copper (hydr)oxychlorides. As discussed previously, the epoxy or OH groups were found to be involved in the formation of bonds with the inorganic phase.[9,19]

The EDX analysis of the composite surfaces reveals interesting results. The maps of elements and the content of those elements on the surface in atomic % are presented in Figure 3 and Table 2, respectively. In both samples chlorine is detected in a significant quantity, especially for CuGr adding to the complexity of the inorganic phase. This also suggests that sodium hydroxide was not able to react stoichiometrically with all copper present in our system and chloride is retained in the form of complexes on the surface. Interestingly, more chlorine is present on the surface of CuGr than on CuGO; however, in the case of the latter sample, its dispersion on the surface seems to be more uniform. As expected, the total exfoliation of GO results in more carbon and much less copper visible on the surface of CuGO than on that of CuGr. Those differences in copper accessibility/presence on the surface and speciation can affect the performance as adsorbents of hydrogen sulfide. An important difference is in the surface ratio of Cu/O, which is 5 for CuGr and only 0.65 and 0.67 for CuGO and CuO−C, respectively. This suggests that copper on the surface of CuGr is in more reduced state and such a high ratio may be indicative of the metallic copper nanoparticles dispersed on the surface of

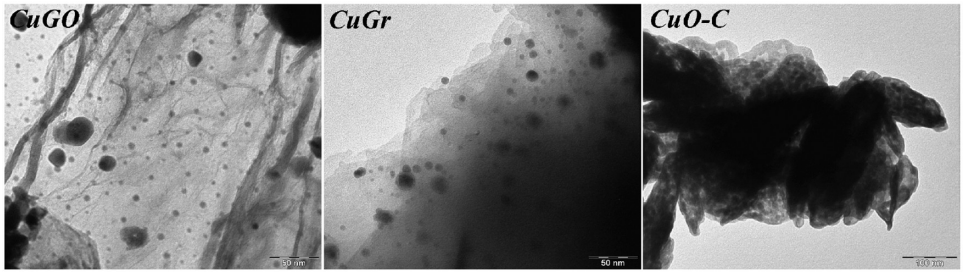

Figure 2. TEM images for the materials studied.

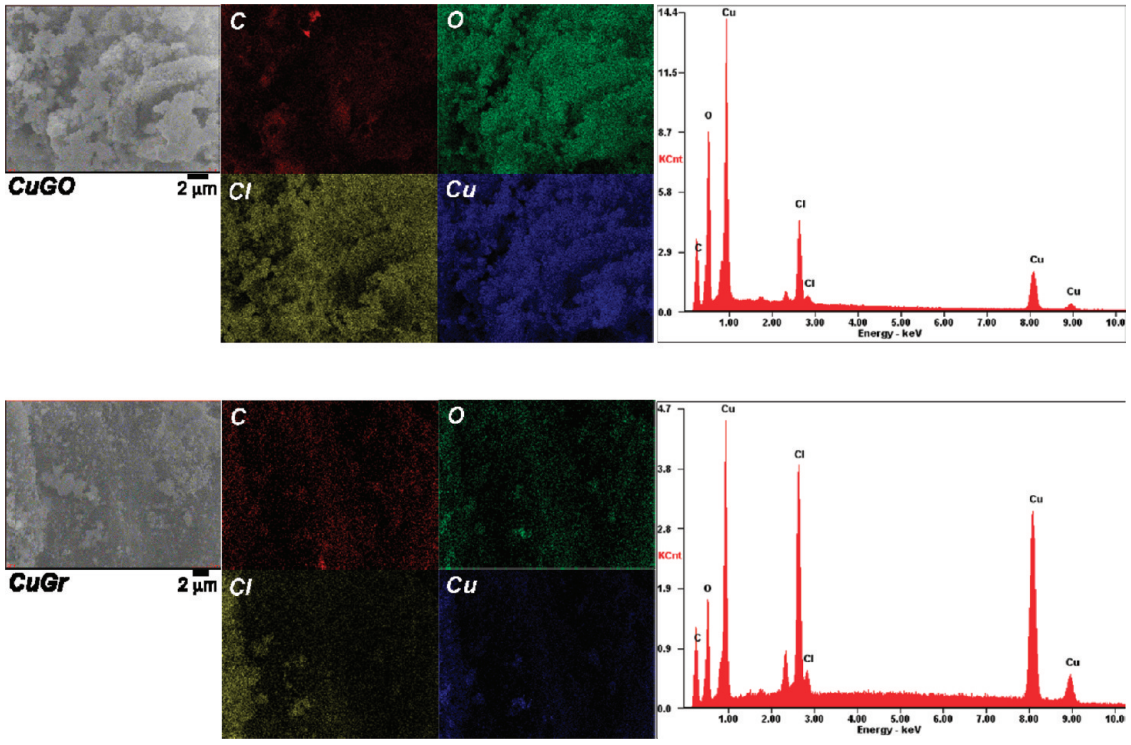

Figure 3. EDX maps of elements.

Table 2. Content of Elements (C, O, Cl, Cu) in Atomic % in the Materials Studied

	at %			
sample	C	O	Cl	Cu
CuGO	42.3	31.0	6.3	20.4
CuGr	29.0	10.7	9.0	51.3
CuO-C		60.0		40.0

this composite. A direct proof for the existence of this kind of nanoparticle requires further research.

The X-ray diffraction experiments are an important mean for the evaluation of the chemistry and structure of our composites. The diffraction patterns for the initial and spent samples are collected in Figure 4. As seen, the materials significantly differ in their degree of crystallinity. The composite with graphene shows the well-defined crystallographic phases of $Cu_2(OH)_3Cl$ (16.25, 18.95, 30.91, 32.47, 39.92, 50.30, and 53.74°) and CuO (38.42 and 44.67°). The peak from stacked graphene layers is also seen at 2 theta 26.49° with interlayer distance (3.36 Å).[19] Interestingly, no metallic copper is detected which suggests its very high dispersion on the surface. The characteristic peaks corresponding to copper chloride hydroxides are in agreement with the ones reported in literature.[33,34] Lee et al. linked the diffraction peaks located at 2 theta 16.25 and 39.79° to both $Cu_2(OH)_3Cl$ and $Cu(OH)_2$.[35] Apparentl,y in the case of CuGO the graphene oxide phase is very well dispersed since the peak at d_{002} characteristic for GO is not revealed. This composite looks much more amorphous than CuGr and at 2 theta about 16° two sharp diffraction peaks are seen at 15.51 ° and 16.25°. They are not detected on other materials studied. The presence of hydroxyl groups in GO can result in formation new crystallographic phases of Cu(OH)Cl (15.5 , 34.74, and 37.40°) and $Cu_2(OH)_3Cl$ (16.25, 32.39, and 39.92°).[33,36] The nanoscale copper oxide exhibits peaks characteristic to $Cu(OH)_2*H_2O$.[37] Apparently, commercial copper oxide is in the partially hydrated state. Cu(OH)Cl and $Cu_2(OH)_3Cl$ detected on the surface are Lewis acids and their interaction with water can contribute to the acidic pH values and could account for the reactivity of the moist samples (H_3O^+ reacting with H_2S).[24]

After exposure to hydrogen sulfide, the positions and intensities of the peaks on the diffractogram for CuGr are not significantly affected signifying retention of its crystallographic structure and the lack of its involvement in hydrogen sulfide reactive adsorption. In fact, from the point of view of

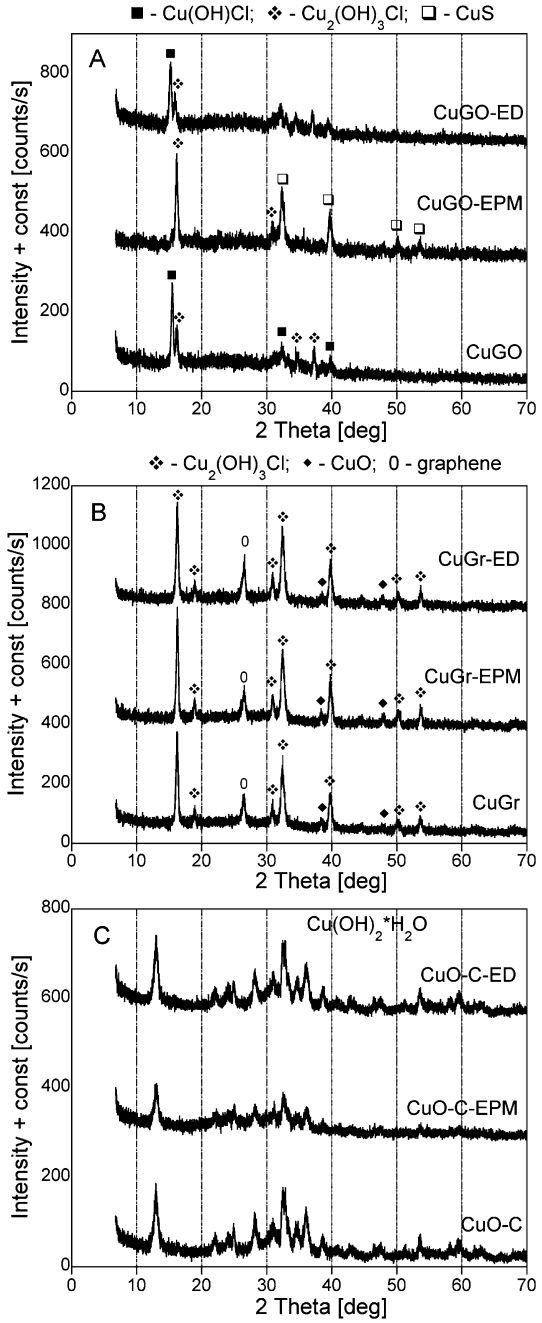

Figure 4. X-ray diffraction patterns for the initial and spent samples: (A) CuGO; (B) CuGr; (C) CuO-C.

reactivity, the amorphous phase of the composites is expected to be more involved in surface reactions than that deposited as well-defined crystals. On the other hand, in the case of CuGO-EPM, a visible difference in diffraction patterns are noticed with the appearance of new peaks at 2θ = 32.34, 39.75, 50.25, and 53.60°. This new pattern represents the formation of crystallographic phase of copper sulfide (CuS)[38] during reactive adsorption. Instead of the split peak at about 16° (presence of Cu(OH)Cl and $Cu_2(OH)_3Cl$), only one peak related to $Cu_2(OH)_3Cl$ is revealed, which supports the hypothesis about the involvement of the chloride phase in reaction with hydrogen sulfide. For commercial copper oxide after adsorption of H_2S in moist conditions, the X-ray diffraction pattern indicates the decrease in the crystallinity level, likely as a result of the formation of amorphous salts.

The comparison of the DTG curves for the initial and spent materials is presented in Figure 5. For the CuO−C,

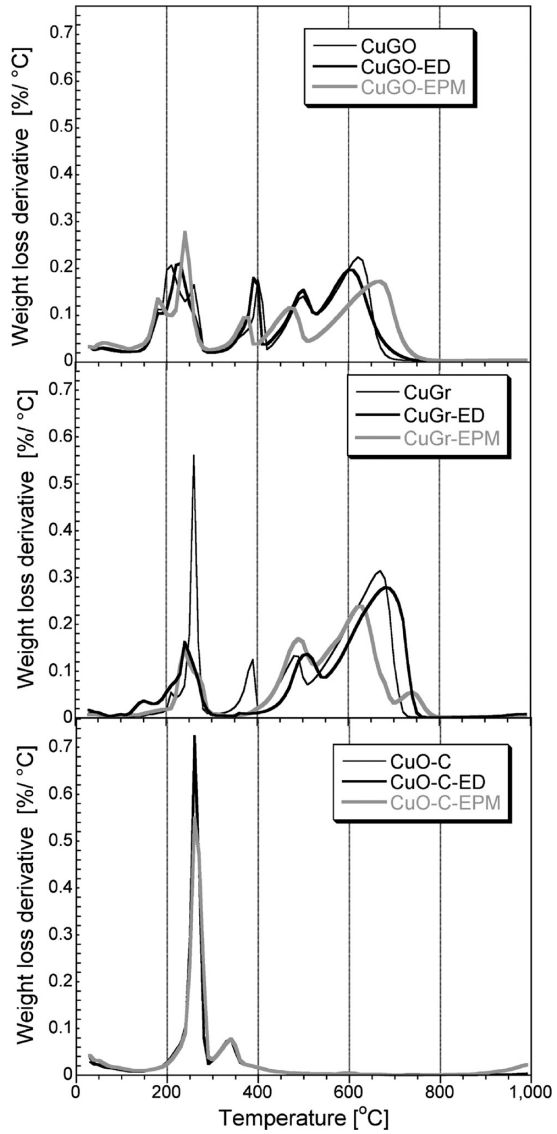

Figure 5. DTG curves in nitrogen for the initial and spent samples.

dehydration and residual dehydroxylation peaks are visible at 260 and 350 °C, respectively. The first peak might also represent the decomposition of carbonates formed from atmospheric CO_2.[39,40] After adsorption of hydrogen sulfide, no changes are detected because of the small adsorption capacity on this material. When the thermal decomposition patterns are compared for the composites the visible differences in surface chemistry are detected. For CuGO the sharp peaks at 200, 260, 400, 500, and 620 °C are visible. Although the first one can be linked to the decomposition of residual epoxy groups of GO[1,7] the second one at 260 °C represents the removal of water of hydration. Then at about 400 °C dehydroxylation is observed. At this temperature also disproportionation of $CuCl_2$ (to Cl_2 and Cu_2Cl_2) is expected.[41] The peaks at 500 and 620 °C are likely related to the two-step reduction of CuO to Cu_2O and then to metallic copper by the carbon phase.[42] Even though this process is expected to take

dx.doi.org/10.1021/am300702a | ACS Appl. Mater. Interfaces 2012, 4, 3316−3324

place at 800−900 °C,[42,43] the presence of copper oxide in the form of small nanoparticles shifts this process to a lower temperature range. The presented above EDX results suggest that metallic copper is formed on the surface of CuGr at room temperature as a result of the contact of small copper oxide nanoparticles with the graphene layers. The difference between the two composites is in the relative intensity of the copper reduction peaks. Although CuGr has much more water of hydration, which is in agreement with its hydrophilic character, the peak representing dehydroxylation on this composite is much less intense than on CuGO suggesting higher contribution of copper oxide and copper in the reduced state to the inorganic phase of this material. Moreover, when the relative intensity of the copper reduction peaks is compared, the results suggest that in CuGr more Cu_2O is present than in CuGO. This could be the effect of the high dispersion of the copper oxide phase and the reductive effects of the graphene phase. Graphite oxide, because of its high content of oxygen, is not able to reduce copper oxide nanoparticles to the same extent as graphene.

After exposure of the composites to H_2S, either in dry or moist conditions, the intensity of the dehydration peak significantly decreases and a shoulder appears at about 290 °C. Interestingly, dehydroxylation peaks for the spent CuGr samples totally disappear suggesting the involvement of OH groups in H_2S retention.[8,11] Although for CuGr-ED, new small peaks are also seen at 150 and 200 °C, in the case of CuGr-EPM, on which the high adsorption capacity was measured, the weight lost pattern in the temperature range between 500 and 800 °C significantly changes. The new intense peak is revealed at about 640 °C and the small one at about 750 °C. Taking into account that sulfides, sulfites, and sulfates can be the products of surface reactions,[44] and based on their decomposition temperature, the later one can be assigned to the reduction of Cu_2O and the former to the decomposition and reduction of copper sulfate, which is expected at 650 °C.[45] Reduction of unreacted copper oxide can also contribute to the weight loss at this temperature range. The complex peak between 200 and 300 °C might represent decomposition of CuS (220 °C), Cu_2SO_3 (200 °C), and $Cu_2SO_3.CuSO_3{\cdot}2H_2O$ (200 °C).[45] For the formation of copper sulfate or sulfite, the oxidation of hydrogen sulfide is needed; it may happen as a result of the ability of copper to activatee oxygen[30,31] that is submitted to the system with the air stream. The oxidized graphene phase can also contribute to this process.[46,47] Exposure of CuGO to hydrogen sulfide in moist air results in a new intense peak at about 220 °C linked to the decomposition of copper sulfide. Then the dehydroxylation peak at about 380 °C decreases in its intensity, which once again is an indication of the involvement of OH groups in surface reactions. The weight loss pattern in dry conditions changes only slightly, which can be linked to relatively small amount of H_2S adsorbed.

The interpretation of the changes in the weight loss can be linked to the changes in the heat effects observed on the DTA curves collected in Figure 6. Although no visible changes are detected on commercial CuO because of the small amount adsorbed, the DTA curves for the spent composites differ from those for the initial samples. For the CuGO the exothermic peak of epoxy groups decomposition is followed by the endothermic effect of dehydration of copper (hydr)-oxychlorides. Then at 400 °C, the exothermic peak of dehydroxylation appears. For the spent samples, especially those exposed to H_2S in most conditions, the endothermic peak

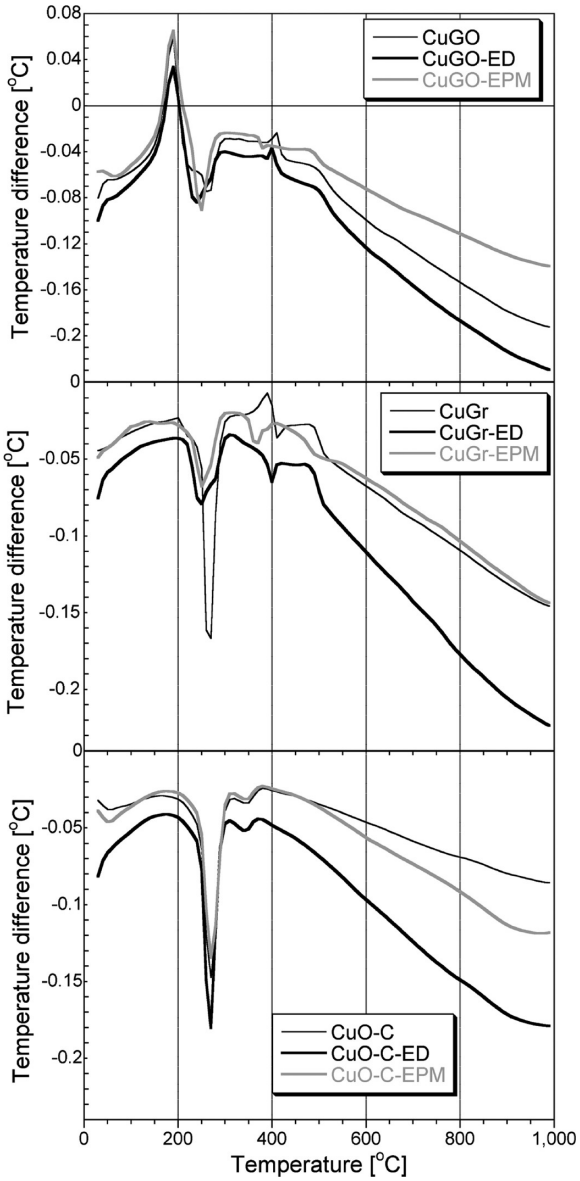

Figure 6. DTA curves in nitrogen for the initial and spent samples.

of the removal of copper sulfides and sulfates appears at about 220 °C, which is followed by a small endothermic peak at about 390 °C. The latter might reflect the removal of HS^-. Those ions likely substituted some OH groups in the (hydr)-oxychlorides lattice. The heat effects are much more pronounced for CuGr where for the initial sample two exothermic peaks at about 400 and 500 °C appear. Taking into account the contribution of copper to the formation of active oxygen and possible oxidation of the graphene phase in the composite by that oxygen, we link the latter effect to the decomposition of oxygen groups (carboxylic) from the surface of the graphene phase. After H_2S adsorption, especially in moist conditions, the endothermic peaks at about 220, 380, and 390 °C are revealed and the heat effects related to dehydroxylation disappear. We link these effects to the removal and melting of sulfur containing salts present on the surface.

The FTIR spectra of the initial and spent materials are presented in Figure 7. Intense bands seen on the spectra for CuO-C samples at 1500 and 1400 cm^{-1} are related to the Cu−O−C stretching of carbonates.[40] As discussed earlier, copper

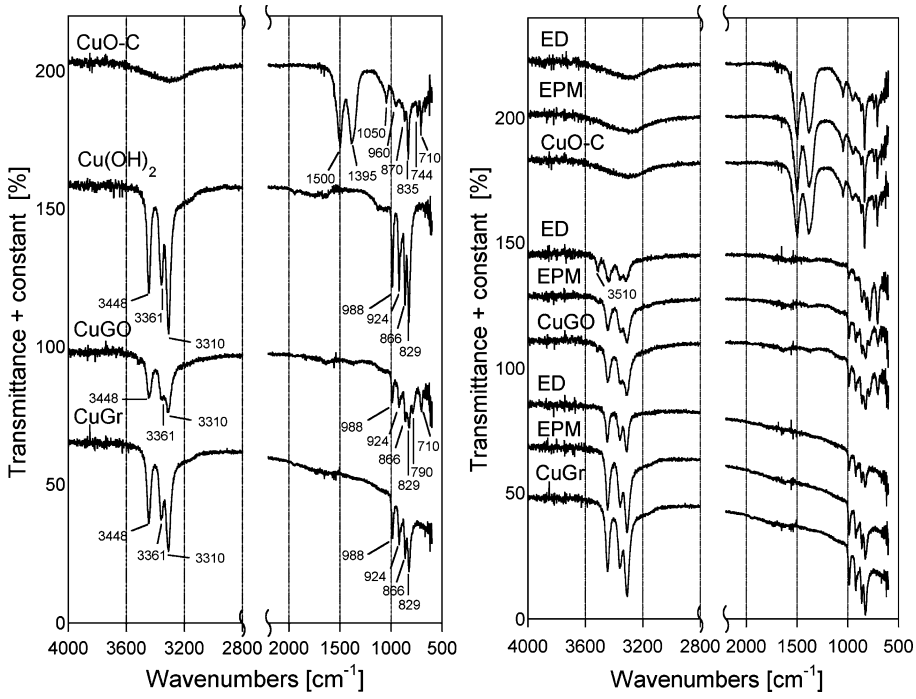

Figure 7. FTIR spectra for the initial and spent samples.

oxide and hydroxide, based on thermal decomposition, might also contain varying amounts of carbonates.[39,40] The numerous bands detected on IR spectra of the composites in the range of 4000−600 cm^{-1} can be linked to the number of different Cu−O and Cu−Cl bond lengths in the $Cu_2(OH)_3Cl$ structure.[48] Cu−OH librations modes appear at wavelengths between 800 and 1000 cm^{-1} for both Gr and GO containing composites (988, 924, 866, and 829 cm^{-1}). They represent the in-plane and out of plane vibrations of four different nonequivalent hydroxyl groups bonded to copper atoms.[43,48] Only three distinct peaks are observed at higher wavelengths at 3348, 3361, and 3310 cm^{-1} corresponding to OH vibration modes of Cu−OH. Those bands are more intense for CuGr than those for CuGO, which can be linked to the higher crystallinity level of the former composite. In addition to the bands described above, two additional bands are seen for the CuGO at 790 and 710 cm^{-1}. Because these bands are not revealed on the spectra for either CuGr or $Cu(OH)_2$, they must be related to interactions between copper and the oxygen groups of graphite oxide. The interactions between Cl and C, although they cannot be completely crossed out, are rather not expected. Cu−O and Cu−Cl vibrations are expected at lower wave numbers (less than 500 cm^{-1}).[43,49] After exposure to H_2S the intensities of the bands representing vibrations of OH groups significantly decreased, which is in agreement with the thermal analysis results. In the case of CuGO-ED, a new band at 3510 cm^{-1} appears and the bands at about 700 and 750 cm^{-1} significantly increase in their intensity. These latter bands represent vibrations of SO_4^{-2} and SO_3^{-2}.[50] An increase in the intensity of the band at 3510 cm^{-1} at dry conditions might be the result of the appearance of water as the product of surface reactions/salt formation.

For the performance of materials as adsorbents, the porosity and accessibility of active centers is of paramount importance. The surface areas of our composites are 8 and 13 m^2/g for CuGO and CuGr, respectively. The materials have the low volume of micropores (0.006 and 0.010 cm^3/g for CuGO and CuGr, respectively) and high volume of mesopores (corresponding values are 0.036 and 0.052 cm^3/g). Since mainly reactive adsorption is responsible for the measured adsorption capacity, the microporosity is not the crucial factor determining the performance. Nevertheless, the CuGr is more porous than CuGO and this might also contribute to its high adsorption capacity.

Potentiometric titration results further support the hypothesis formulated above. As seen on the pK_a distributions (Figure 8) the initial CuGO sample is much more acidic than CuGr. The total numbers of acidic groups are 2.55 and 1.03 mmol/g, respectively. Especially the difference is visible at pK_a about 11.2 where the terminal hydroxyl groups dissociate. Although on the surface of CuGO, 1.73 mmol/g of those species are present, on the CuGr, only 0.66 mmol/g are detected. This is in agreement with the copper being in more reduced state in the latter sample. After H_2S adsorption the terminal OH groups totally disappeared in the case of CuGr-EPM and their number significantly decreased for CuGO-EPM, as detected from thermal analysis. Interestingly on the surface of CuGr-EPM the well-defined peak is detected at pK_a 5.7 (1.67 mmol/g). It is at the position of the carboxylic acid dissociation constant[51] and we linked it to the oxidation of graphene surface by O^{2-}. Highly dispersed copper species and the time factor (aging) likely contributed to this process.

The results presented suggest that the form of graphene-based phase used in the composite determines the chemistry of the active copper (hydr)oxychlorides/copper oxide/metallic copper nanoparticle phase. The water is apparently very important for surface reactions because its ability to dissociate hydrogen sulfide. Even though the pK_{a1} of the hydrogen sulfide in the bulk phase is 7.2, it was demonstrated that in nanospace of porous materials it can dissociate at pH about 4.5.[29] Therefore the copper sulfides are formed on the surface via a direct replacement of the hydroxyl groups of $Cu(OH)_2$. Since either copper nanoparticles[30,31] or graphene phase are able to activate oxygen[46,47] the oxysulfur acids are formed. Those acids

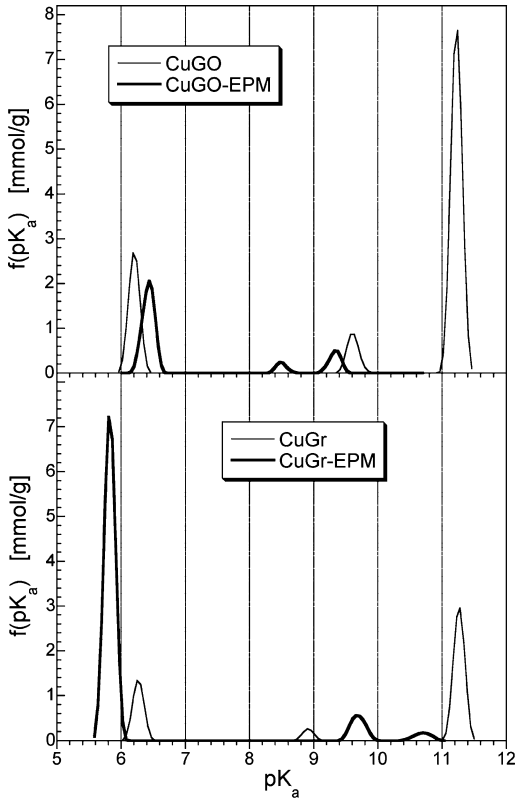

Figure 8. pK_a distributions for the initial composites and those exposed to H_2S in moist conditions.

react either with Cu^{2+} or Cu^{1+} forming sulfites and sulfates. Oxidation of metallic copper also takes place and sulfuric acid can be considered as an oxidant. It was reported that for very small metallic copper particles water can also act as an oxidant.[31] Formation of Cu^{2+} in the water phase can significantly increase the H_2S retention capacity. The oxysulfur acids can also react directly with the $Cu(OH)_2$ replacing its OH groups. The total consumption of the hydroxyls in the case of CuGr is linked to their smaller number than in the case of CuGO and to the presence of more active copper. That active copper helps in formation of more H_2SO_4, which leads to more sulfates. In dry conditions, the dissociation of hydrogen sulfide is limited and formation of sulfides by a direct replacement of terminal hydrated OH groups is the predominant mechanism. More chloride in the case of CuGr also favors the formation of sulfides. Even though in this reaction HCl can be released, as a strong acid, it is expected to react with an excess of available copper hydroxide sites. Graphite oxide and graphene phase can help in electron transfer for redox reactions. Because the graphene phase is expected to be more conductive than GO the reactive adsorption is more efficient. The carboxylic groups existing at the edges of the flakes are not expected to decrease conductivity significantly. The nanoparticles of copper species visible on the surface of the composites provide the effective contact of H_2S or sulfur oxyacids with the active copper. Moreover, EDX results suggest that on the surface of CuGr more copper sites are available for contact with hydrogen sulfide. Also, the particles are smaller and thus more copper can be in effective contact with H_2S, water and oxygen. The porosity of the composites, although almost not existing, should not be totally neglected.

CONCLUSIONS

The presented results showed that the composite with graphene has the more favorable surface features enhancing reactive adsorption of hydrogen sulfide than the composite with graphite oxide. On it, almost 16 wt % H_2S can be removed in the dynamic condition used in our experimental approach. The amount adsorbed at equilibrium can be even higher. This good performance is linked to the high dispersion of copper species on the surface in the reduced state. This copper contributes to oxidation of the graphene phase and an increase in its hydrophilicity and porosity. The presence of moisture in the gas phase has a positive effect on the removal process owing to the dissociation process. H_2S is retained on the surface via a direct replacement of OH groups and via acid−base reactions with the copper (hydr)oxychlorides. Highly dispersed reduced copper species nanoparticles on the surface of the composite with graphene enhance activation of oxygen and cause formation of sulfites and sulfates. The presence of chlorides was also indicated as beneficial for surface reactivity. Higher conductivity of the graphene phase than that of graphite oxide helps in electron transfer in redox reactions. That strong positive effect of highly dispersed copper species in the composite with graphene on the retention of hydrogen sulfide at ambient conditions might also prove to be beneficial for other TICs removal on the visible-light-active composites as those with zinc hydroxides when the mixed oxide phase is employed as an active phase.

AUTHOR INFORMATION

Corresponding Author

*Tel: +1 212 650 6017. Fax: +1 212 650 6107. E-mail: tbandosz@ccny.cuny.edu.

Notes

The authors declare no competing financial interest.

ACKNOWLEDGMENTS

This work was supported by ARO Grant W911NF-10-1-0039, NSF collaborative grant CBET 1133112, and PSC−CUNY Grant 63098-0041. Experimental help of Mr. Neel Patel is highly appreciated

REFERENCES

(1) Stankovich, S.; Dikin, D. A.; Piner, R. D.; Kohlhaas, K. A.; Kleinhammes, A.; Jia, Y.; Wu, Y.; Nguyen, S. T.; Ruoff, R. S. *Carbon* **2007**, *45*, 1558−1565.
(2) Williams, G.; Serger, B.; Kamat, P. V. *ACS Nano* **2008**, *2*, 1487−1491.
(3) Xu, C.; Wang, X.; Yang, L.; Wu, Y. *J. Solid State Chem.* **2009**, *182*, 2486−2490.
(4) Yang, S. T.; Chang, Y.; Wang, H.; Liu, G.; Chen, S.; Wang, Y.; Liu, Y.; Cao, A. *J. Colloid Interface Sci.* **2010**, *351*, 122−127.
(5) Chandra, V.; Park, J.; Chun, Y.; Lee, J. W.; Hwang, I.-C.; Kim, K. S. *ACS Nano* **2010**, *4*, 3979−3986.
(6) Chandra, V.; Kim, K. S. *Chem. Commun.* **2011**, *47*, 3942−3944.
(7) Petit, C.; Seredych, M.; Bandosz, T. J. *J. Mater. Chem.* **2009**, *19*, 9176−9185.
(8) Seredych, M.; Bandosz, T. J. *Chem. Eng. J.* **2011**, *166*, 1032−1038.
(9) Seredych, M.; Bandosz, T. J. *J. Phys. Chem. C* **2010**, *114*, 14552−14560.
(10) Bashkova, S.; Bandosz, T. J. *Ind. Eng. Chem. Res.* **2009**, *48*, 10884−10891.
(11) Seredych, M.; Mabayoje, O.; Bandosz, T. J. *Langmuir* **2012**, *28*, 1337−1346.

(12) Matsuo, Y.; Nishino, Y.; Fukutsuka, T.; Sugie, Y. *Carbon* **2008**, *46*, 1162−1163.
(13) Morishige, K.; Hamada, T. *Langmuir* **2005**, *21*, 6277−6281.
(14) Zhao, Y.; Ding, H.; Zhong, Q. *Appl. Surf. Sci.* **2012**, *258*, 4301−4307.
(15) Levasseur, B.; Petit, C.; Bandosz, T. J. *ACS Appl. Mater. Interfaces* **2010**, *2*, 3606−3613.
(16) Petit, C.; Bandosz, T. J. *Adv. Funct. Mater.* **2010**, *20*, 111−118.
(17) Seredych, M.; Mabayoje, O.; Bandosz, T. J. Manuscript in preparation.
(18) Seredych, M.; Mabayoje, O.; Bandosz, T. J. *J. Phys. Chem. C* **2012**, *116*, 2527−2535.
(19) Seredych, M.; Mabayoje, O.; Koleśnik, M. M.; Krstić, V.; Bandosz, T. J. *J. Mater. Chem.* **2012**, *22*, 7970−7978.
(20) Shin, H.-J.; Sim, K. K.; Benayad, A.; Yoon, S.-M.; Park, H. K.; Jung, I.-S.; Jin, M. H.; Jeong, H.-K.; Kim, J. M.; Choi, J.-Y.; Lee, Y. H. *Adv. Funct. Mater.* **2009**, *19*, 1987−1992.
(21) Bagreev, A.; Bandosz, T. J. *Carbon* **2001**, *39*, 2303−2311.
(22) Mabayoje, O.; Seredych, M.; Bandosz, T. J. *J. Colloid Interface Sci.* **2012**, *378*, 1−9.
(23) Huang, C. C.; Chen, C. H.; Chu, S. M. *J. Hazard. Mater.* **2006**, *136*, 866−873.
(24) Polychronopoulou, K.; Galisteo, F. C.; López Granados, M.; Fierro, J. L. G.; Bakas, T.; Efstathiou, A. M. *J. Catal.* **2005**, *236*, 205−220.
(25) Dhage, P.; Samokhvalov, A.; Repala, D.; Duin, E. C.; Bowman, M.; Tatarchuk, B. J. *Ind. Eng. Chem. Res.* **2010**, *49*, 8388−8396.
(26) Jagiello, J. *Langmuir* **1994**, *10*, 2778−2785.
(27) Jagiello, J.; Bandosz, T. J.; Schwarz, J. A. *Carbon* **1994**, *32*, 1026−1028.
(28) Dubinin, M. M. In *Chemistry and Physics of Carbon*; Walker, P. L., Ed.; Marcel Dekker: New York, 1966; Vol. 2, p 51.
(29) Bandosz, T. J. *J. Colloid Interface Sci.* **2002**, *246*, 1−20.
(30) Kobayashi, M.; Flytzani-Stephanopoulos, M. *Ind. Eng. Chem. Res.* **2002**, *41*, 3115−3123.
(31) Nguyen-Thanh, D.; Bandosz, T. J. *Carbon* **2005**, *43*, 359−367.
(32) Lerf, A.; He, H.; Fosrter, M.; Klinowski, J. *J. Phys. Chem B* **1998**, *102*, 4477−4482.
(33) Zheng, X. G.; Kawae, T.; Kashitani, Y.; Li, C. S.; Tateiwa, N.; Takeda, K.; Yamada, H.; Xu, C. N.; Ren, Y. *Phys. Rev. B: Condens. Matter. Mater. Phys.* **2005**, *71*, 052409 (4 pages).
(34) Elzey, S.; Baltrusaitis, J.; Bian, S.; Grassian, V. H. *J. Mater. Chem.* **2011**, *21*, 3162−3169.
(35) Lee, S. C.; Park, S. H.; Lee, S. M.; Lee, J. B.; Kim, H. J. *Catal. Today* **2007**, *120*, 358−362.
(36) Cudennec, Y.; Riou, A.; Gerault, Y.; Lecerf, A. *J. Solid State Chem.* **2000**, *151*, 308−312.
(37) Cudennec, Y.; Lecerf, A.; Riou, A.; Gerault, Y. *Eur. J. Solid State Inorg. Chem.* **1990**, *27*, 411−417.
(38) Takeuchi, Y.; Kudoh, Y.; Sato, G. *Z. Kristallogr.* **1985**, *173*, 119−128.
(39) Shaheen, W. M.; Maksod, I. H. A. E. *J. Alloys Compd.* **2009**, *476*, 366−372.
(40) Soler-Illia, G. J. A.; Candal, R. J.; Regazzoni, A. E.; Blesa, M. A. *Chem. Mater.* **1997**, *9*, 184−191.
(41) Ramamurtahnyde, P.; Secco, A. *Can. J. Chem.* **1969**, *47*, 2185−2190.
(42) Inagaki, M.; Okada, Y.; Miura, K.; Konno, H. *Carbon* **1999**, *37*, 329−334.
(43) García-Martínez, O.; López Delgado, A.; Millán, P.; López, S.; Rojas, R. M.; Ligeras, P. *Calorim. Anal. Therm.* **1985**, *XVI*, 350−357.
(44) Bandosz, T. J. In *Activated Carbon Surfaces in Environmental Remediation*; Bandosz, T. J., Ed.; Elsevier: Oxford, U.K., 2006; p 231.
(45) Weast, R. C.; Astle, M. J. In *Handbook of Chemistry and Physics*, 62nd ed.; Weast, R. C., Astle, M. J., Eds.; CRC Press: Boca Raton, FL, 1981; p B−99.
(46) Strelko, V. V.; Kartel, N. T.; Dukhno, I. N.; Kuts, V. S.; Clarkson, R. B.; Odintsov, B. M. *Surf. Sci.* **2004**, *548*, 281−290.
(47) Stohr, B.; Boehm, H. P. *Carbon* **1991**, *29*, 707−720.
(48) Stoilova, D.; Vassileva, V. *C.R. Acad. Bulg. Sci.* **2002**, *55*, 51−54.
(49) Du, A.; Zhou, B.; Shen, J.; Xiao, S.; Zhang, Z.; Liu, C.; Zhang, M. *J. Non-Cryst. Solids* **2009**, *355*, 175−181.
(50) Bohner, U.; Zundel, G. *J. Phys. Chem.* **1985**, *89*, 1408−1413.
(51) Kortum, G.; Vogel, W.; Andrusso, K. *Dissociation Constants of Organic Acids in Aqueous Solutions*; Butterworth: London, 1961.